

We are IntechOpen, the world's leading publisher of Open Access books Built by scientists, for scientists

6,000

Open access books available

148,000

International authors and editors

185M

Downloads

Our authors are among the

154

Countries delivered to

TOP 1%

most cited scientists

12.2%

Contributors from top 500 universities



WEB OF SCIENCE™

Selection of our books indexed in the Book Citation Index
in Web of Science™ Core Collection (BKCI)

Interested in publishing with us?
Contact book.department@intechopen.com

Numbers displayed above are based on latest data collected.
For more information visit www.intechopen.com



Ghost Diffraction Holography: A Correlation Assisted Quantitative Tool for Complex Field Imaging and Characterization

Vinu Raveendran Pillai Vasantha Kumari, Ziyang Chen, Rakesh Kumar Singh and Jixiong Pu

Abstract

The fascinating domain of ghost imaging has been a subject of interest in the fundamental and applied research for the last two decades with its promising applications in various imaging and characterization scenarios. In this chapter, we discuss the recently developed ghost diffraction holography (GDH) system with due emphasis on the capability of quantitative complex-field imaging in the ghost framework. The development of the unconventional correlation-assisted GDH technique by adopting the holography concept in ghost diffraction scheme is described, and the quantitative phase imaging capability is demonstrated in the microscopy. In addition, the technique exploits the spatial statistics of time-frozen recorded speckle intensity with snapshot detection in ghost framework, which could broaden the applications of the developed microscopy to real-time imaging of two- and three-dimensional biological samples with high resolution. Furthermore, we discuss demonstrated applications of the technique in the imaging various spatially varying complex-valued macroscopic and microscopic samples and the potential application of the technique in the recovery and characterization of orbital angular momentum modes encoded in spatially incoherent speckle field.

Keywords: ghost imaging, ghost diffraction, digital holography, digital holographic microscopy, speckles, quantitative phase imaging, orbital angular momentum

1. Introduction

Optical imaging relying on ghost approaches has been emerged as a novel imaging modality with the superior capability of high-resolution complex-valued image restoration that the traditional approaches cannot match even in the imaging scenarios with chaotic or turbulent environment [1–4]. Last two decades witnessed the theoretical and applied advancements in ghost imaging (GI) modalities from quantum to classical to computational approaches by utilizing the cross-correlation of intensity measurements in spatial, temporal or spectroscopy domains [5–11]. The counterintuitive imaging

modality of ghost schemes acquire the high-resolution ghost image by exploiting the cross-correlation of intensities of object interacted scattered field detected by a single pixel detector and a field that never interacted with the object detected by a multi pixel detector. Since the first observance of ghost effect by Belenskii and Klyshko in 1994 [12] and later the experimental demonstration by Pittmann in 1995 [13] with entangled light from a spontaneous parametric down conversion source, numerous advancements have been reported by making use of various light sources and different correlation protocols. Besides the initial discussion over the quantum versus classical nature of the GI [14], the demonstration of pseudo-thermal light source in place of the parametric down conversion source opens the door for the development of more applied imaging techniques [15, 16]. Later the progress in the computational techniques and the introduction of computational GI [9] paves the path for the development of several techniques exploiting the advanced algorithms such as compressive sensing [17], deep learning [18, 19], differential measurement [20, 21], sequential deviation [22], etc. In recent years, researchers exploited the fascinating features of ghost schemes in other realms of applied imaging with cutting edge technological demonstrations of ghost tomography [23], ghost spectroscopy [8], X-ray ghost imaging [24, 25], temporal GI [7], electron GI [26], GI with atoms [27], etc.

Alongside the significant developments of GI techniques in high-resolution image restoration, the classical framework of GI schemes encounters the challenges of pure phase object imaging, which significantly limits the applications in biomedical imaging. Owing to the phase imaging challenge in GI framework, a few approaches utilizing ghost diffraction (GD) [28, 29], phase retrieval algorithms [30], interferometry schemes [31–34], Fourier-space filtering [35], and phase-shifting digital holography [34], etc. has been demonstrated in recent years. Most of the demonstrated phase imaging techniques in ghost schemes emphasis on low spatially varying phase objects, and demands the sophisticated measuring setups, time sequential detection of large set of sampling data, high quality reconstruction algorithm, etc. for the faithful phase recovery. In addition, the real-time quantitative phase imaging applications with ghost schemes demands the requirement of phase recovery from an instantaneous or time frozen intensity recordings. In this chapter we describe our recently invented technique of ghost diffraction holography (GDH) [36–38], where the quantitative phase recovery in a ghost system is made possible by adopting the concept of off-axis holography in combination with the conventional ghost diffraction system. The technique utilizes a snapshot recording scheme with synchronized detectors and exploits the spatial statistics of time frozen speckle field from a pseudo-thermal light source for the correlation of intensity fluctuations. In the following sections we describe different features of GDH system by giving emphasis on the snapshot detection scheme in GD system, recovery of complex correlation function, extension of GDH to a ghost diffraction holographic microscopy (GDHM) system, and finally on the recovery and characterization of orbital angular momentum modes (OAM) using a GDH system.

2. Classical framework of ghost diffraction system

In the last two decades GI and GD techniques has been emerged as well-established optical imaging techniques, which exploits the intensity correlations to obtain an image or diffraction pattern of an object, respectively. The realization of classical counterpart of the ghost schemes with entangled source open the door for the

utilization of various light sources and thereby by the execution of the approach in various applied imaging scenarios where the conventional imaging techniques limits in the performance [14–16]. The classical ghost schemes perform coherent imaging with spatially incoherent light by make use of the intensity correlations of identical spatially correlated beams, one of them interact with the object, while the other has never interacted with the object. To understand the classical framework of ghost diffraction scheme, let us consider the conceptual schematic of a ghost diffraction system as shown in **Figure 1**. The stochastic field emanating from the spatially incoherent source is divided in to two identical copies by a beam splitter, where one of the fields reaches the detector, D1 after illuminating an object, while the other field reaches detector, D2 without interacting with the object. A conventional GD system uses a point detector as D1 in the object arm and a multipixel detector as D2 in the reference arm. For a stochastic process that obeys Gaussian statistics, the cross-correlation of spatial intensity fluctuations of object field and reference field retrieves the diffraction pattern of the object [16], which is expressed as

$$G = \langle \Delta I_o(\mathbf{r}_1) \Delta I_r(\mathbf{r}_2) \rangle = |\mathbf{g}^{(G)}(\mathbf{r}_1, \mathbf{r}_2)|^2 \quad (1)$$

where $\langle \dots \rangle$ represents the ensemble averaging, $I_o(\mathbf{r}) = |u_o(\mathbf{r})|^2$ and $I_r(\mathbf{r}) = |u_r(\mathbf{r})|^2$ are the intensity values at the detectors of object field ($u_o(\mathbf{r})$) and reference field ($u_r(\mathbf{r})$), respectively with $\Delta I(\mathbf{r}) = I(\mathbf{r}) - \langle I(\mathbf{r}) \rangle$ representing the spatial intensity fluctuation with respect to its average value, \mathbf{r} the position coordinate in the detector plane and $\mathbf{g}^{(G)}(\mathbf{r}_1, \mathbf{r}_2) = \langle u_o^*(\mathbf{r}_1) u_r(\mathbf{r}_2) \rangle$ is the ghost diffraction correlation function that represents the diffraction pattern of the object.

The cross-correlation of intensity fluctuations implemented in the GD scheme directly retrieves only the modulus of the cross-correlation function or diffraction pattern of the object. This limits the direct and simultaneous recovery of phase along with the amplitude of the object, which restricts the execution of ghost schemes in complex-valued object imaging. A few GI schemes are demonstrated in recent years on considering the significance of optical phase imaging by utilizing the phase retrieval techniques or by using other indirect experimental schemes. Owing to the phase recovery challenges in ghost schemes, we have recently developed a GDH system by adopting the off-axis holography scheme in combination with the

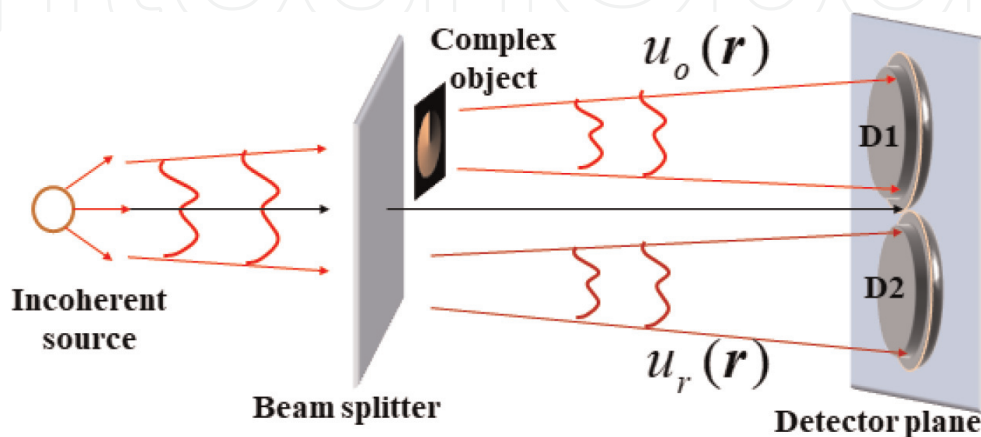


Figure 1. Conceptual schematic of classical ghost diffraction system. Adapted with permission from [36] © The Optical Society.

conventional GD system. Section 3 describes in detail the GDH system and its extension to the microscopy for quantitative complex field imaging.

3. Ghost diffraction holography

The GDH combines the holographic concept with the conventional ghost diffraction scheme for the simultaneous quantitative phase and amplitude imaging. A conceptual schematic of the GDH scheme is shown in **Figure 2**, where a reference random field generated from an independent source is mixed with the fields emanating from the conventional GD system. The cross-correlation of spatial intensity fluctuations at the respective detectors retrieves a correlation hologram in the intensity correlation function. The digital processing of the correlation hologram recovers the complex correlation function, and thereby make possible the complex-valued object imaging. In comparison to conventional GD approaches, the GDH utilizes snapshot detection scheme by utilizing the time-frozen speckle field from a pseudothermal light source by considering the ergodicity in space.

3.1 Snapshot GDH based on spatial averaging

The GDH system utilizes the holographic addition of the reference random field $u_R(\mathbf{r})$ generated from an independent source with the object field $u_o(\mathbf{r})$ and reference field $u_r(\mathbf{r})$ of the conventional ghost diffraction system [36–38]. Therefore, the resultant intensity distributions at the respective detectors are given by,

$$\begin{aligned} I_o(\mathbf{r}) &= (u_o(\mathbf{r}) + u_R(\mathbf{r}))^* (u_o(\mathbf{r}) + u_R(\mathbf{r})) \\ I_r(\mathbf{r}) &= (u_r(\mathbf{r}) + u_R(\mathbf{r}))^* (u_r(\mathbf{r}) + u_R(\mathbf{r})) \end{aligned} \quad (2)$$

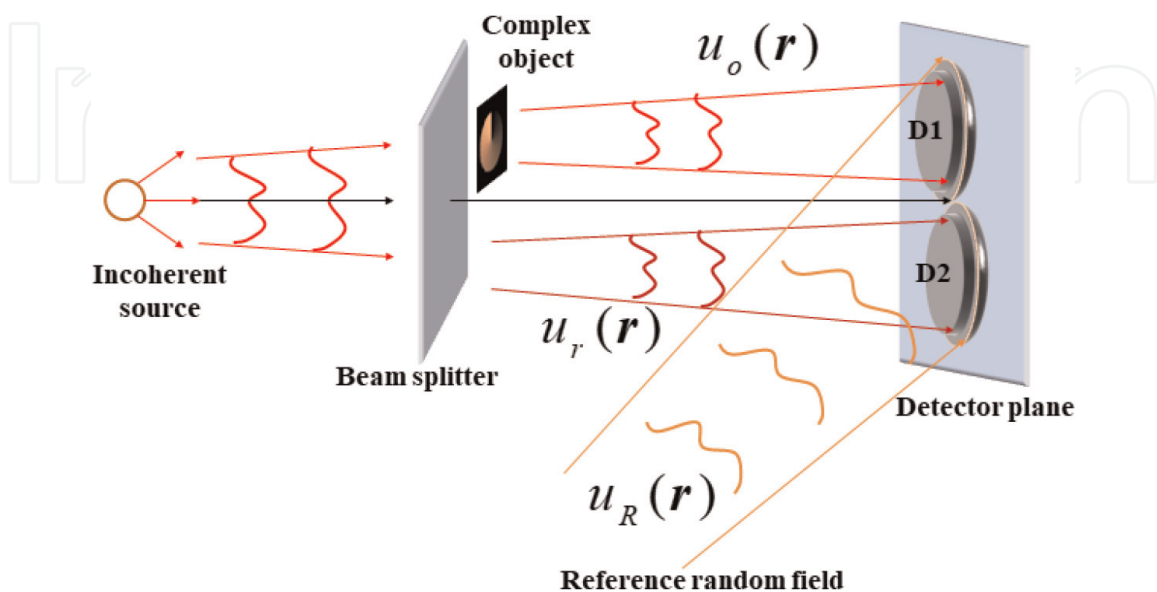


Figure 2. Conceptual schematic of ghost diffraction holography (GDH) system. The GDH system utilizes a rotating ground glass diffuser as a spatially incoherent source. Adapted with permission from [36] © The Optical Society.

where the field distributions at the respective detectors are expressed as

$$\begin{aligned}
 u_o(r) &= \frac{\exp(ikz)}{i\lambda z} \int u_o(\hat{r}) \exp(i\varphi_g(\hat{r})) T(\hat{r}) \exp\left[\frac{ik}{2z} (|r|^2 - 2r \cdot \hat{r} + |\hat{r}|^2)\right] d\hat{r} \\
 u_r(r) &= \frac{\exp(ikz)}{i\lambda z} \int u_o(\hat{r}) \exp(i\varphi_g(\hat{r})) \exp\left[\frac{ik}{2z} (|r|^2 - 2r \cdot \hat{r} + |\hat{r}|^2)\right] d\hat{r} \\
 u_R(r) &= \frac{\exp(ikz)}{i\lambda z} \int u_R(\hat{r}) \exp(i\varphi_R(\hat{r})) \exp\left[\frac{ik}{2z} (|r|^2 - 2r \cdot \hat{r} + |\hat{r}|^2)\right] d\hat{r}
 \end{aligned} \tag{3}$$

with ' λ ' the wavelength of light source, $\varphi_g(\hat{r})$ and $\varphi_R(\hat{r})$ are the random phase introduced by the rotating ground glass diffuser in the GD system and the reference ground glass diffuser, respectively, ' $k = 2\pi/\lambda$ ' the wave number, ' z ' the propagation distances in the respective arms, $T(\hat{r})$ is the transmittance function of the object, and \hat{r} and r are the position coordinate in the diffuser plane and detector plane, respectively.

The ghost schemes utilize the cross-correlation of spatial intensity fluctuations at the respective detector plane, which is expressed as:

$$G = \langle \Delta I_o(\mathbf{r}_1) \Delta I_r(\mathbf{r}_2) \rangle \tag{4}$$

where $\langle \dots \rangle$ represents the ensemble averaging, $\Delta I_o(\mathbf{r}_1) = I_o(\mathbf{r}_1) - \langle I_o(\mathbf{r}_1) \rangle$ and $\Delta I_r(\mathbf{r}_2) = I_r(\mathbf{r}_2) - \langle I_r(\mathbf{r}_2) \rangle$ represents the fluctuation of the intensity value with respect to its average value for the respective intensity distributions at the detectors. On assuming the scattered field from the diffusers obeys Gaussian statistics and by utilizing the fourth order moment of the field at the detectors, the cross-correlation of intensity fluctuations in Eq. (4) is related to the respective second order correlation function as [39, 40]:

$$\begin{aligned}
 \langle \Delta I_o(\mathbf{r}_1) \Delta I_r(\mathbf{r}_2) \rangle &= |\langle (u_o(\mathbf{r}_1) + u_R(\mathbf{r}_1))^* (u_r(\mathbf{r}_2) + u_R(\mathbf{r}_2)) \rangle|^2 \\
 &= |\langle u_o^*(\mathbf{r}_1) u_r(\mathbf{r}_2) + u_o^*(\mathbf{r}_1) u_R(\mathbf{r}_2) + u_R^*(\mathbf{r}_1) u_r(\mathbf{r}_2) + u_R^*(\mathbf{r}_1) u_R(\mathbf{r}_2) \rangle|^2 \\
 &= |\langle u_o^*(\mathbf{r}_1) u_r(\mathbf{r}_2) \rangle + \langle u_R^*(\mathbf{r}_1) u_R(\mathbf{r}_2) \rangle|^2 \\
 &= |g^G(\mathbf{r}_1, \mathbf{r}_2) + g^R(\mathbf{r}_1, \mathbf{r}_2)|^2
 \end{aligned} \tag{5}$$

where $g^G(\mathbf{r}_1, \mathbf{r}_2) = \langle u_o^*(\mathbf{r}_1) u_r(\mathbf{r}_2) \rangle$, and $g^R(\mathbf{r}_1, \mathbf{r}_2) = \langle u_R^*(\mathbf{r}_1) u_R(\mathbf{r}_2) \rangle$ are the second order correlation functions corresponding to the ghost diffraction field and the reference random field from the holographic arm, respectively. Here, the contribution from the cross terms is taken as zero. i.e., $\langle u_o^*(\mathbf{r}_1) u_R(\mathbf{r}_2) \rangle = \langle u_R^*(\mathbf{r}_1) u_r(\mathbf{r}_2) \rangle = 0$, since independent diffusers are used to generate the respective random fields.

The execution of ensemble averaging in the correlation process can be performed either with the temporal averaging or with the spatial averaging. In view of the real-time implementation of the ghost schemes with quantitative phase imaging potential, the GDH system rely on spatial averaging by considering the time frozen speckle fields at the detector plane under the assumption of spatial stationarity [41, 42]. A snapshot detection scheme in GDH is implemented by replacing the point detector of a conventional GD system with a multi pixel detector D1, which is synchronized with another multi pixel detector D2. The spatial averaging operation on the detected intensity distributions is carried out by fixing the distance $\Delta \mathbf{r} = \mathbf{r}_1 - \mathbf{r}_2$ equivalent to

the pixel size at the detector plane, and by moving a specific window size in the intensity distribution $I_o(r)$ over the entire intensity image $I_r(r)$. On applying a change of variables $r_1 = r + \Delta r$ and $r_2 = r$ with $\Delta r = r_1 - r_2$, the Eq. (5) modifies to

$$\begin{aligned} G &= \langle \Delta I_o(r + \Delta r) \Delta I_r(r) \rangle \\ &= |g^G(r + \Delta r, r) + g^R(r + \Delta r, r)|^2 \end{aligned} \quad (6)$$

where $g^G(r + \Delta r, r)$ represents the complex field correlation function that encodes the diffraction pattern of the object, which can be further expressed as.

$$\begin{aligned} g^G(r + \Delta r, r) &= \langle u_o^*(r + \Delta r) u_r(r) \rangle \\ &= \frac{1}{\lambda^2 z^2} \iint u_o^*(\hat{r}_1) T(\hat{r}_1) u_o(\hat{r}_2) \delta(\hat{r}_1 - \hat{r}_2) \exp\left(-i(\varphi_g(\hat{r}_1) - \varphi_g(\hat{r}_2))\right) \\ &\quad \exp\left(-i\frac{k}{2z}(|\hat{r}_1|^2 - |\hat{r}_2|^2)\right) \times \exp\left(-i\frac{2\pi}{\lambda z} \Delta r \cdot \hat{r}_1\right) d\hat{r}_1 d\hat{r}_2 \end{aligned} \quad (7)$$

with $\delta(\hat{r}_1 - \hat{r}_2) \propto \int \exp(-i\frac{2\pi}{\lambda z}(\hat{r}_1 - \hat{r}_2) \cdot r) dr$ the delta function. The contributions corresponding to the r dependent phase factors $\exp\left(ik\frac{|r|^2}{2z}\right)$ and $\exp\left(ik\frac{|r+\Delta r|^2}{2z}\right)$ were canceled out while estimating the cross correlation of intensity fluctuations as in Eq. (6). On considering $\hat{r}_2 = \hat{r}_1 = \hat{r}$ and $u_o^*(\hat{r})u_o(\hat{r}) = I_o(\hat{r})$, the Eq. (7) modifies to

$$g^G(\Delta r) = \frac{1}{\lambda^2 z^2} \int I_o(\hat{r}) T(\hat{r}) \exp\left(-i\frac{2\pi}{\lambda z} \Delta r \cdot \hat{r}\right) d\hat{r} \quad (8)$$

Similarly, the reference correlation function $g^R(r + \Delta r, r)$ in the Eq. (6) results into

$$\begin{aligned} g^R(r + \Delta r, r) &= \langle u_R^*(r + \Delta r) u_R(r) \rangle \\ &= \frac{1}{\lambda^2 z^2} \iint u_R^*(\hat{r}_1) u_R(\hat{r}_2) \delta(\hat{r}_1 - \hat{r}_2) \exp(-i(\varphi_R(\hat{r}_1) - \varphi_R(\hat{r}_2))) \exp\left(-i\frac{k}{2z}(|\hat{r}_1|^2 - |\hat{r}_2|^2)\right) \\ &\quad \times \exp\left(-i\frac{2\pi}{\lambda z} \Delta r \cdot \hat{r}_1\right) d\hat{r}_1 d\hat{r}_2 \end{aligned} \quad (9)$$

On considering $\hat{r}_2 = \hat{r}_1 = \hat{r}$ and $u_R^*(\hat{r})u_R(\hat{r}) = I_R(\hat{r})$ at the reference diffuser plane, Eq. (9) modifies to

$$g^R(\Delta r) = \frac{1}{\lambda^2 z^2} \int I_R(\hat{r}) \exp\left(-i\frac{2\pi}{\lambda z} \Delta r \cdot \hat{r}\right) d\hat{r} \quad (10)$$

By substituting Eqs. (8) and (10) in Eq. (4), the intensity correlation function in terms of the position vector Δr is expressed as

$$\begin{aligned} G &= \langle \Delta I_o(r + \Delta r) \Delta I_r(r) \rangle = |g^G(\Delta r) + g^R(\Delta r)|^2 \\ &= \left| \frac{1}{\lambda^2 z^2} \left\{ \int I_o(\hat{r}) T(\hat{r}) \exp\left(-i\frac{2\pi}{\lambda z} \Delta r \cdot \hat{r}\right) d\hat{r} + \int I_R(\hat{r}) \exp\left(-i\frac{2\pi}{\lambda z} \Delta r \cdot \hat{r}\right) d\hat{r} \right\} \right|^2 \end{aligned} \quad (11)$$

Eq. (11) describes the cross-correlation of intensity fluctuations in the GDH scheme, which results into the generation of the ghost correlation hologram. In the GDH scheme, the reference correlation function is generated by an off-axis point source illumination on an independent ground glass diffuser with the intensity at the source structure, $I_R(\hat{r}) = \text{circ}\left(\frac{\hat{r}-r_s}{a}\right)$, which is controlled by the position r_s and size a of the aperture used to illuminate the independent reference ground glass diffuser. The $g^R(\Delta r)$ provides a linear phase to generate the ghost correlation hologram, and the size of the aperture is selected in such a way that it covers the extent of $g^G(\Delta r)$. In the GDH system, the recording and reconstruction of the object information is carried out in terms of the coherence functions rather than in terms of the optical field as in the conventional holography system [36, 43–45]. A digital processing in the correlation hologram by making use of Fourier transform method [46], retrieves the complex correlation function $g^G(\Delta r)$ from other redundant terms of the correlation hologram. The complex correlation function retrieval provides the flexible opportunity to recover the complex-valued object information at any specific plane by making use of digital propagation methods [47].

3.2 GDH design

A schematic diagram of the GDH system with snapshot recording scheme is shown in **Figure 3**. The design consists of a conventional ghost diffraction part (Part I), an outer holographic reference arm with an independent random field (Part II) and the snapshot recording and digital processing module (Part III). A coherent light source splitting into two beams by a non-polarizing beam splitter (BS1) act as the source beams for Part I and Part II of the system. The coherent beam transmitting through a rotating ground glass diffuser (GG1) generates the speckle field, which act as the pseudothermal source for the ghost diffraction system. The design utilizes the orthogonal polarized components of light beams by using a polarization beam splitter (PBS1) for the development of a common path snapshot recording of the ghost object and reference fields. The reflected beam from BS1 generates a reference random field by allowing the beam to pass through the combination of an off-axis microscope objective and a ground glass diffuser GG2. This reference random field from Part II propagates and combines with the common path propagating orthogonally polarized scattered fields from the Part I of the system using a beam splitter BS2. A snapshot recording scheme is developed by using the combination of two synchronized charge coupled device (CCD) cameras, CCD1 and CCD2 and polarizers P1 and P2 at specific orientations. The polarizers are used for the projection and superposition of corresponding polarization components from Part I and part II of the system with maximum visibility. At a specific instant of time the CCD's records the intensity distributions of superposed object and reference fields.

3.3 Recovery of complex correlation function

The performance of the GDH system (shown in **Figure 3**) for complex correlation function recovery is theoretically and experimentally demonstrated with various pure phase objects and real-valued objects. The pure phase of helical mode with topological charge, $l = 1$ (shown in **Figure 4a**) from a vortex phase plate (VPP) is used as a pure phase object in the experimental design shown in **Figure 3**.

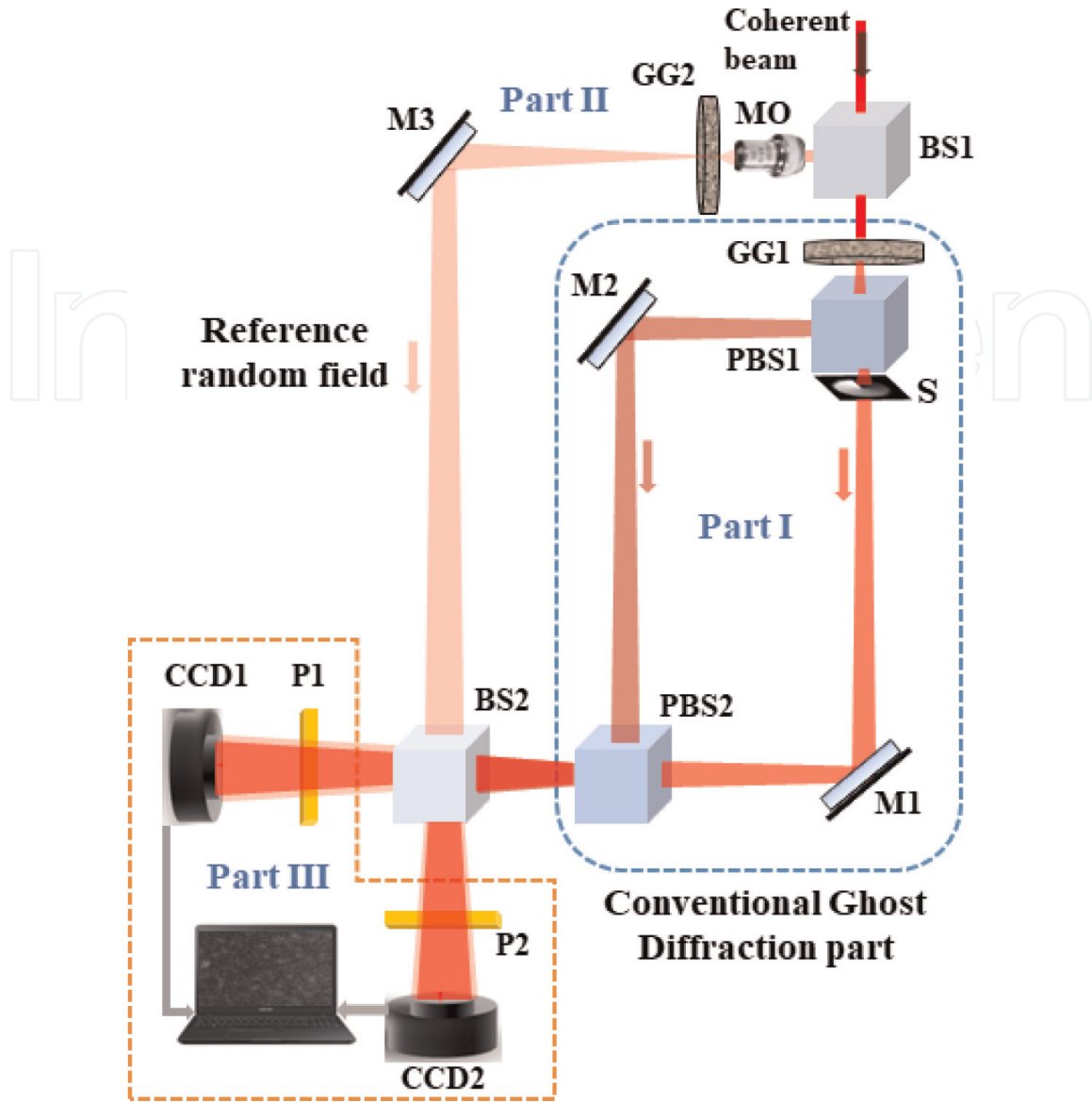


Figure 3. Schematic of the GDH system; part I: Conventional ghost diffraction part, part II: Holographic arm with reference random field, part III: Snapshot recording and digital processing module, BS: Beam splitter, GG: Ground glass diffuser, S: Sample, M: Mirror, PBS: Polarization beam splitter, MO: Microscope objective, P: Polarizer, and CCD: Charge coupled device. Adapted with permission from [36] © The Optical Society.

The snapshot detection scheme records the intensity distribution corresponding to the object and reference fields, which are shown in **Figure 4b** and **Figure 4c**, respectively. The cross-correlation of intensity fluctuations from the two detectors results in a ghost correlation hologram as expressed by Eq. (6) and is shown in **Figure 4d**. The existence of a fork pattern in the ghost correlation hologram clearly indicates the encoding of the phase information in the correlation hologram. A digital analysis based on Fourier transform method [46] of fringe analysis recovers the complex correlation function from the ghost correlation hologram. The recovered amplitude and phase distribution at the detector plane corresponding to the helical mode with $l = 1$ is shown in **Figure 4e** and **f**. Moreover, to illustrate the validity of the system, a GDH system is simulated with helical wavefront $\exp(il\phi)$, where l is the topological charge and ϕ the angular coordinate of the pure phase sample. The simulation of the GDH system is implemented by considering a light source of wavelength 632.8 nm and the beam of specific size like the experimental conditions to illuminate the

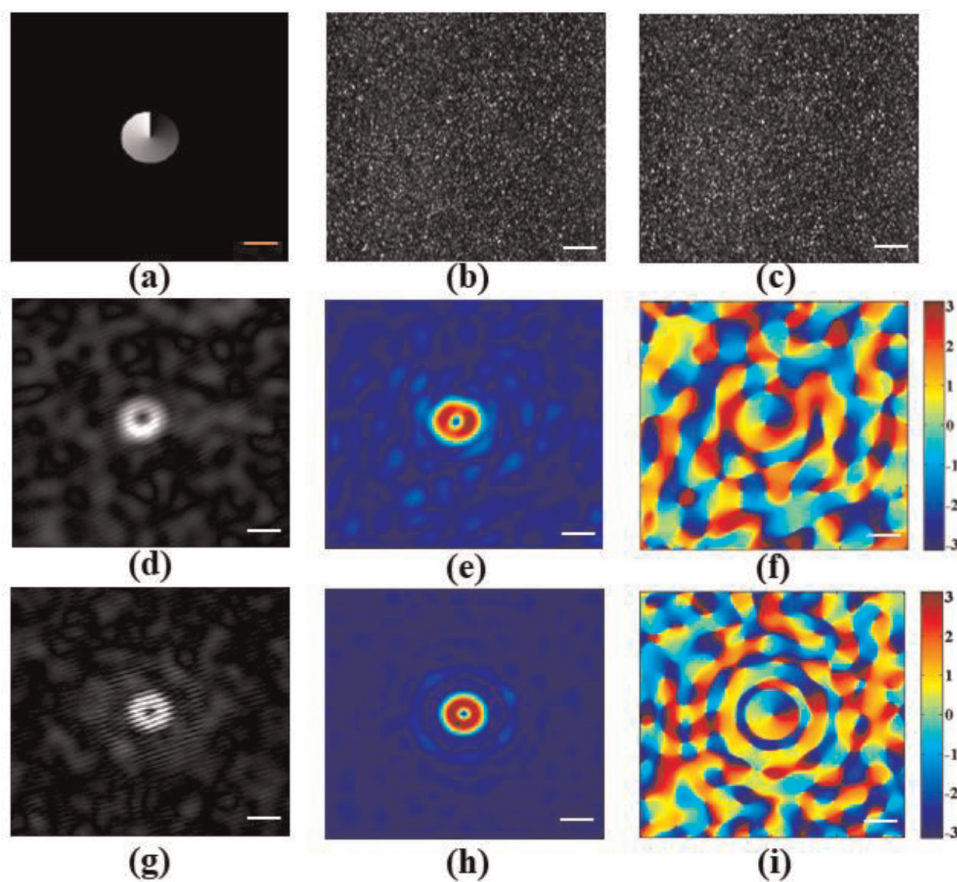


Figure 4. Recovery of complex correlation function for a phase object; (a) pure phase of a helical mode with topological charge 1, (b) & (c) recorded intensity distributions corresponding to the object field and reference fields, (d)–(f) experimental results of ghost correlation hologram, amplitude, and phase distributions of complex correlation functions, respectively, (g)–(i) simulation results of ghost correlation hologram, amplitude, and phase distributions of complex correlation functions, respectively, scale bar: (a) 2.5 mm, (b) & (c) 1.32 mm, and (d)–(i) 138 μm .

rotating diffuser. The reference random field is generated by an off-axis point source illumination on an independent diffuser. The simulation results corresponding to ghost correlation hologram, recovered amplitude and phase distributions are shown in **Figure 4g–i**, respectively.

Furthermore, the ability of the approach in real-valued case is demonstrated with a triangular pattern of aperture (shown in **Figure 5a**) as an object for the experimental design shown in **Figure 3**. The triangular aperture generates off-axis propagating random fields on illuminating the surface with a speckle field from the rotating diffuser. The superposition of three off axis propagating random light beams creates an array of vortices in the complex correlation function [48, 49]. The recorded intensity distributions corresponding to the object field and reference field are shown in **Figure 5b** and **c**, respectively. The cross-correlation of intensity fluctuations of the object field and reference field at the detector plane retrieves the ghost correlation hologram as shown in **Figure 5d**, which clearly has an array of fork fringes in the intensity distribution. A digital processing on the hologram retrieves the complex correlation function. The amplitude and phase distribution of complex correlation function is shown in **Figure 5e** and **f**, which shows an array of dark core and the helical phase distribution corresponding to the dark core in its amplitude and phase distribution, respectively. The experimental results were compared with the simulation results corresponding to a triangular aperture as sample, and the respective

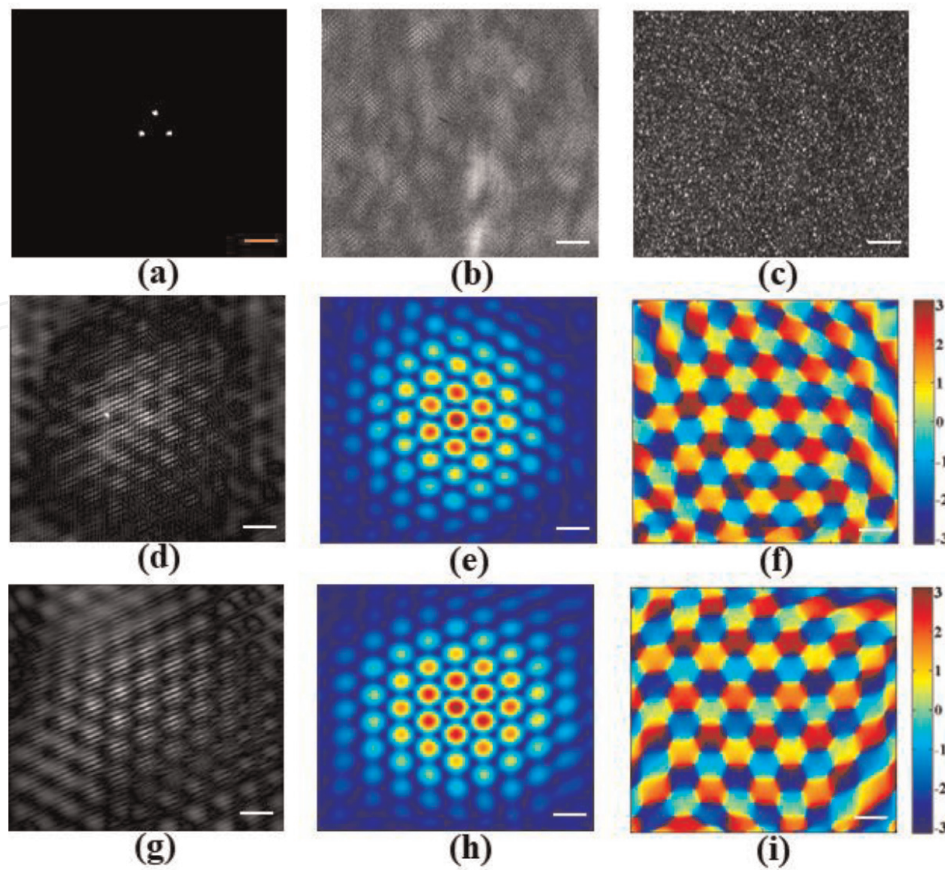


Figure 5. Recovery of complex correlation function for a triangular aperture; (a) pure phase of a helical mode with topological charge 1, (b) & (c) recorded intensity distributions corresponding to the object field and reference fields, (d)–(f) experimental results of ghost correlation hologram, amplitude, and phase distributions of complex correlation functions, respectively, (g)–(i) simulation results of ghost correlation hologram, amplitude, and phase distributions of complex correlation functions, respectively, scale bar: (a) 2.5 mm, (b) & (c) 1.32 mm, and (d)–(i) 138 μm .

results corresponding to ghost correlation hologram, amplitude and phase distributions are shown in **Figure 5g–i**. A good agreement between simulation and experimental results in the recovery of complex correlation function for various objects using GDH provides the potential provision to realize the technique in quantitative imaging of complex-valued object.

3.4 Quantitative phase and amplitude imaging

The complex field correlation function recovery from snapshot detected intensities make the provision to recover the complex-valued image of the object at specific plane by employing a digital beam propagation approach based on angular spectrum method [47]. The digital analysis procedure employed in the technique for the simultaneous quantitative phase and amplitude image recovery of an object is shown in **Figure 6**. The synchronized CCD's records the intensity distribution corresponding to the ghost object field and reference field at a fixed time. A spatial averaging assisted cross-correlation of intensity fluctuations retrieves the ghost correlation hologram at the detector plane. By applying a Fourier transform operation on the ghost correlation hologram, the spectra and its conjugate spectra are separated from the central dc term. The complex correlation function is retrieved by performing an inverse Fourier transform operation on the filtered and centrally shifted spectrum. The simultaneous

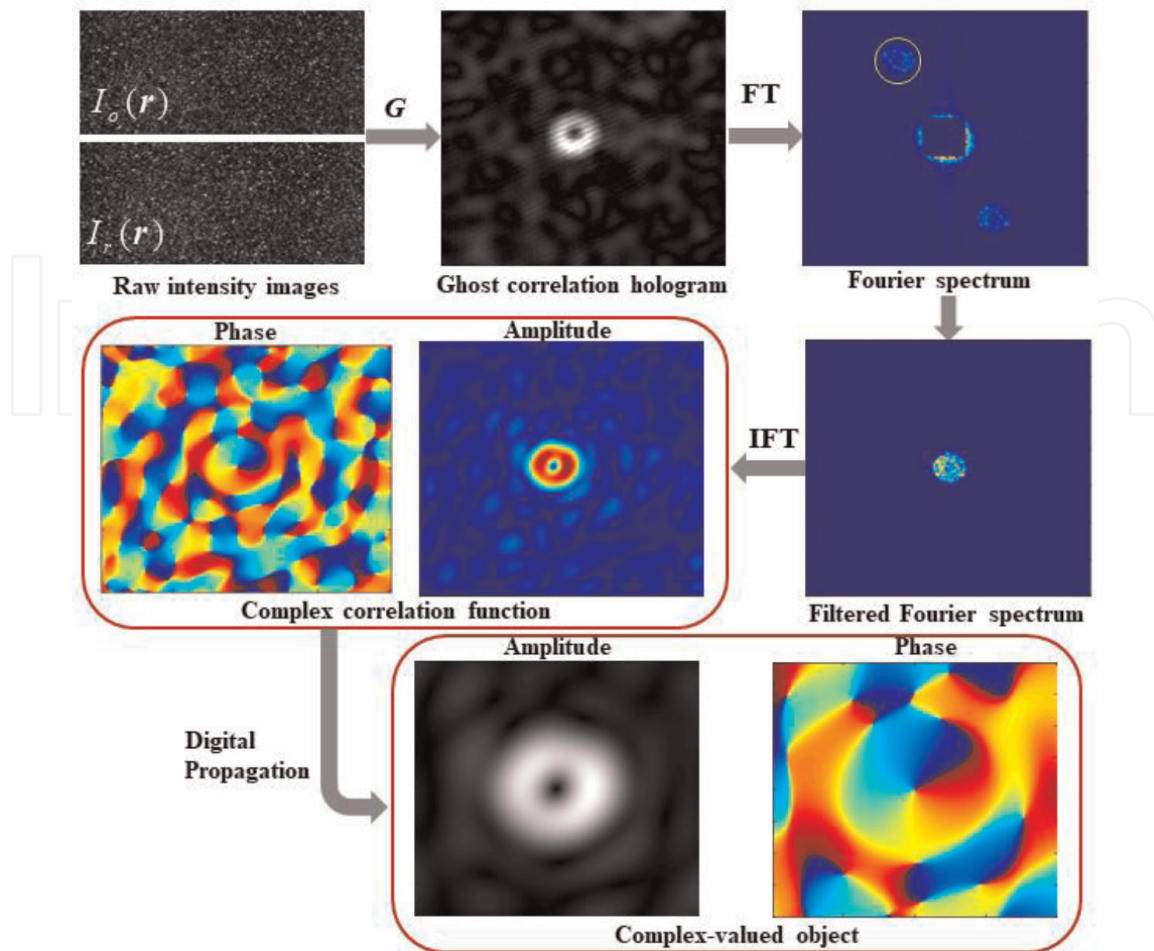


Figure 6. Digital analysis scheme of quantitative phase and amplitude imaging with GDH system; $I_o(r)$ and $I_r(r)$ are the recorded intensity distributions corresponding to the object and reference fields; G : Cross-correlation of intensity fluctuations; FT: Fourier transform, and IFT: Inverse Fourier transform. Adapted with permission from [36] © The Optical Society.

retrieval of amplitude and phase distribution of correlation function make the provision to recover the complex-valued object at the desired plane using angular spectrum method of digital propagation. The performance of the GDH system in complex-valued object imaging is demonstrated with various objects like pure phase object, planar transparency, 1951 USAF resolution test target, etc. The quantitative phase and amplitude imaging of various objects used in the GDH system are shown in **Figure 7**.

3.5 Ghost diffraction holographic microscopy

In view of the significance of the digital holographic microscopy in biomedical imaging, the imaging potential of the GDH system is extended to the domain of microscopy, the GDH microscopy (GDHM) system. An experimental design of the GDHM system is shown in **Figure 8**. The system utilizes identical microscopy configuration in the ghost object and reference field as represented in part I of the **Figure 8**. An adjustable combination of different microscope objectives and tube lenses are utilized in the system according to the dimensions of the sample. The random fields from microscopy assisted ghost object and reference fields superpose with the independent reference field from Part II of the system. The combination of polarizers and CCDs records the intensity distribution corresponding to the polarization components

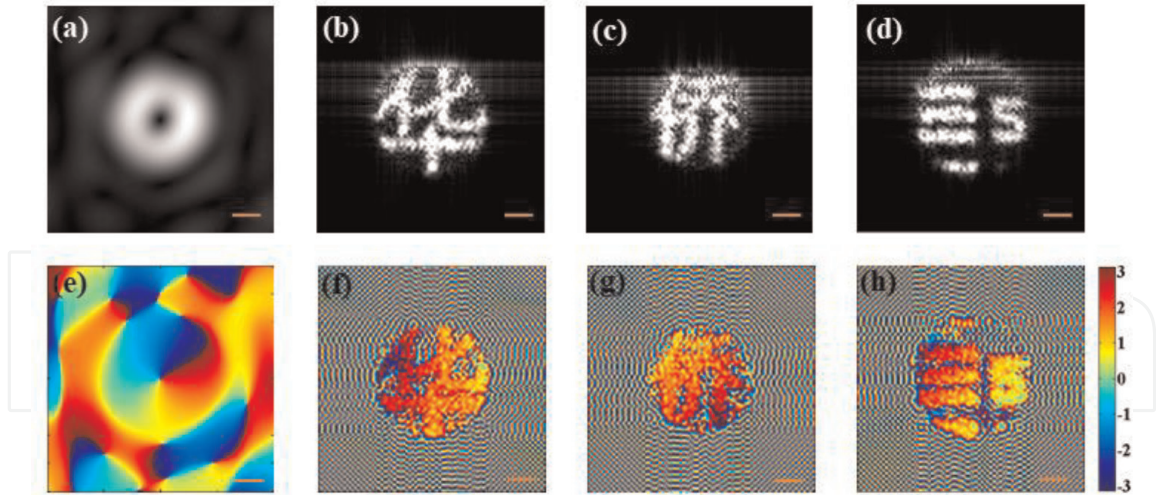


Figure 7.

Quantitative phase and amplitude imaging of various objects with GDH system; first row: Recovered amplitude distributions; second row: Recovered phase distributions; (a) & (e) VPP with $l = 1$; (b) & (f) Chinese character “HUA”; (c) & (g) Chinese character “QIAO”; and (d) & (h) negative 1951 USAF resolution test target. Scale bar: 1.15 mm. Adapted with permission from [36] © The Optical Society.

from different arms. A quantitative comparison of imaging results of USAF 1951 resolution test target with GDH and GDHM system are shown in **Figure 9**. The first two rows in **Figure 9** represent the imaging results of GDH system, where the reconstruction quality deteriorates as it reaches Group-0, Element-4 of the test target. The last two rows in **Figure 9** represent the imaging results corresponding to GDHM system with various configurations of microscope objectives and tube lenses. A detailed quantitative comparison of imaging results is given in **Table 1**. The GDHM system have a good resolving ability up to Group-7, Element-1 with the given experimental design, which corresponds to 128-line pairs/mm with a line width of 3.9 μm (**Table 1**).

4. Recovery and characterization of orbital angular momentum modes

The characteristic feature of the complex correlation function recovery of GDH system is recently exploited to develop a technique for the recovery and characterization of OAM modes [50]. The OAM associated with a vortex electromagnetic wave is an independent physical dimension of light having the characteristics of orthogonality and infinite-dimensional basis, which have remarkable applications in imaging, optical communication, quantum and classical information processing, multidimensional coding, etc. [51–53]. The optical vortex beams carries an OAM equivalent to $l\hbar$ per photon (\hbar is the Planck’s constant divided by 2π) with an azimuthal phase of $\exp(il\phi)$, where l is the topological charge and ϕ the angular coordinate. Last two decades witnessed a tremendous development of various techniques for the generation of vortex beams, and in recent years the research efforts shifting from coherent vortex beams to low coherent light with helical phase modes in partially coherent beams [54–56].

Alongside the progress in the developments of vortex beam generation techniques, a significant number of techniques were introduced for the detection and sorting of various OAM modes [51, 52]. However, most of the conventional detection and

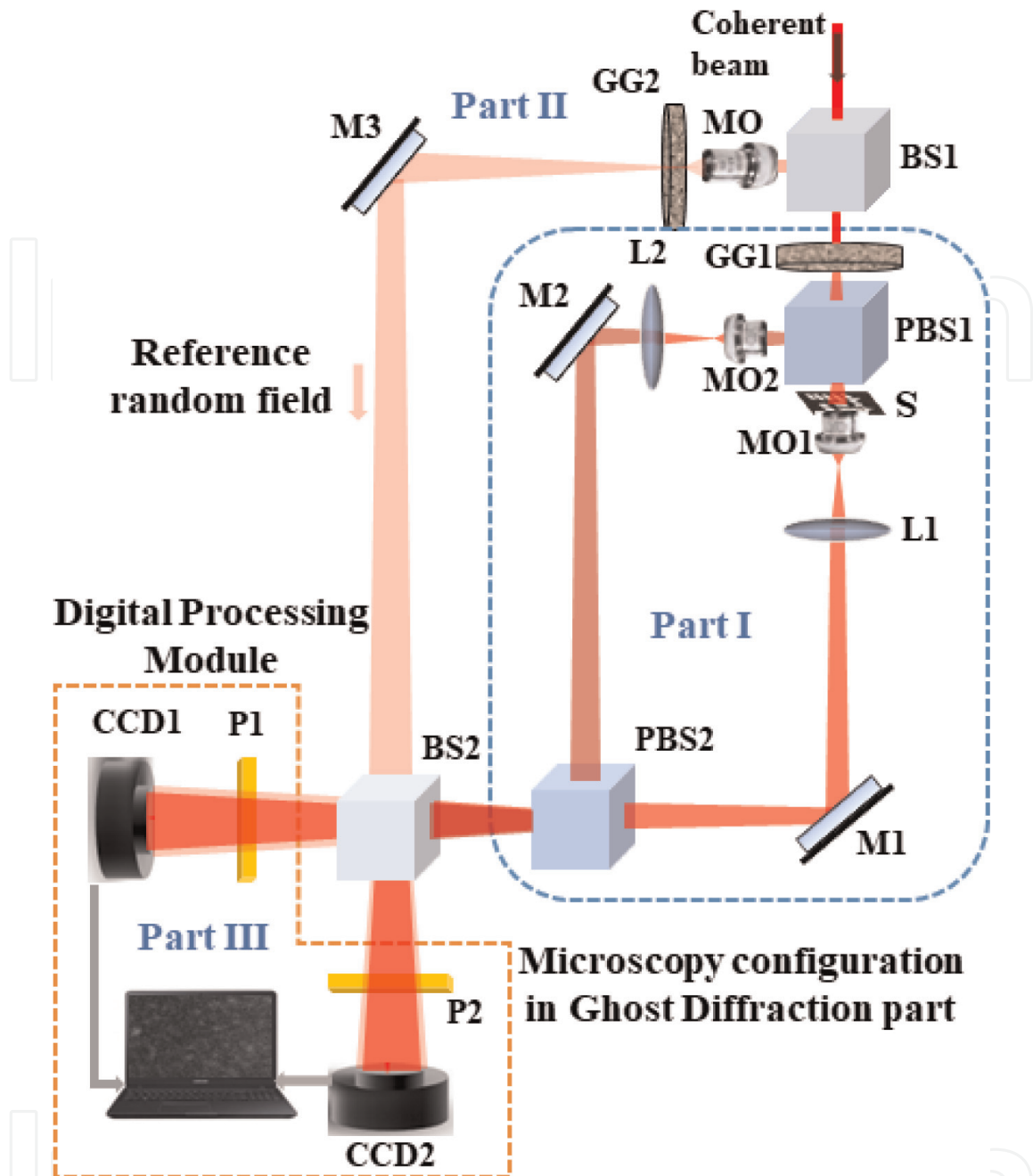


Figure 8. Schematic of the GDHM system; Part I: Conventional ghost diffraction part with microscopy configuration, Part II: Holographic arm with reference random field, part III: Snapshot recording and digital processing module, BS: Beam splitter, GG: Ground glass diffuser, S: Sample, M: Mirror, PBS: Polarization beam splitter, MO: Microscope objective, P: Polarizer, and CCD: Charge coupled device. Adapted with permission from [36] © The Optical Society.

sorting techniques limits its application in scenarios where the propagating medium is inhomogeneous or turbulent in nature, which scrambles the helical wavefront of the vortex beam and destroys the orthogonality. A few research efforts were put forwarded in recent years to tackle the challenges of vortex beam propagation through scattering medium by exploiting the information carrying potential of speckle fields [45, 49, 57–59]. In addition, a few techniques were demonstrated for helicity and topological charge (TC) determination of partially coherent vortex beams [60, 61], robustness investigation of low coherent vortex beam propagation through noisy and turbulent media [62, 63], discrimination of incoherent vortex states of light [64], and

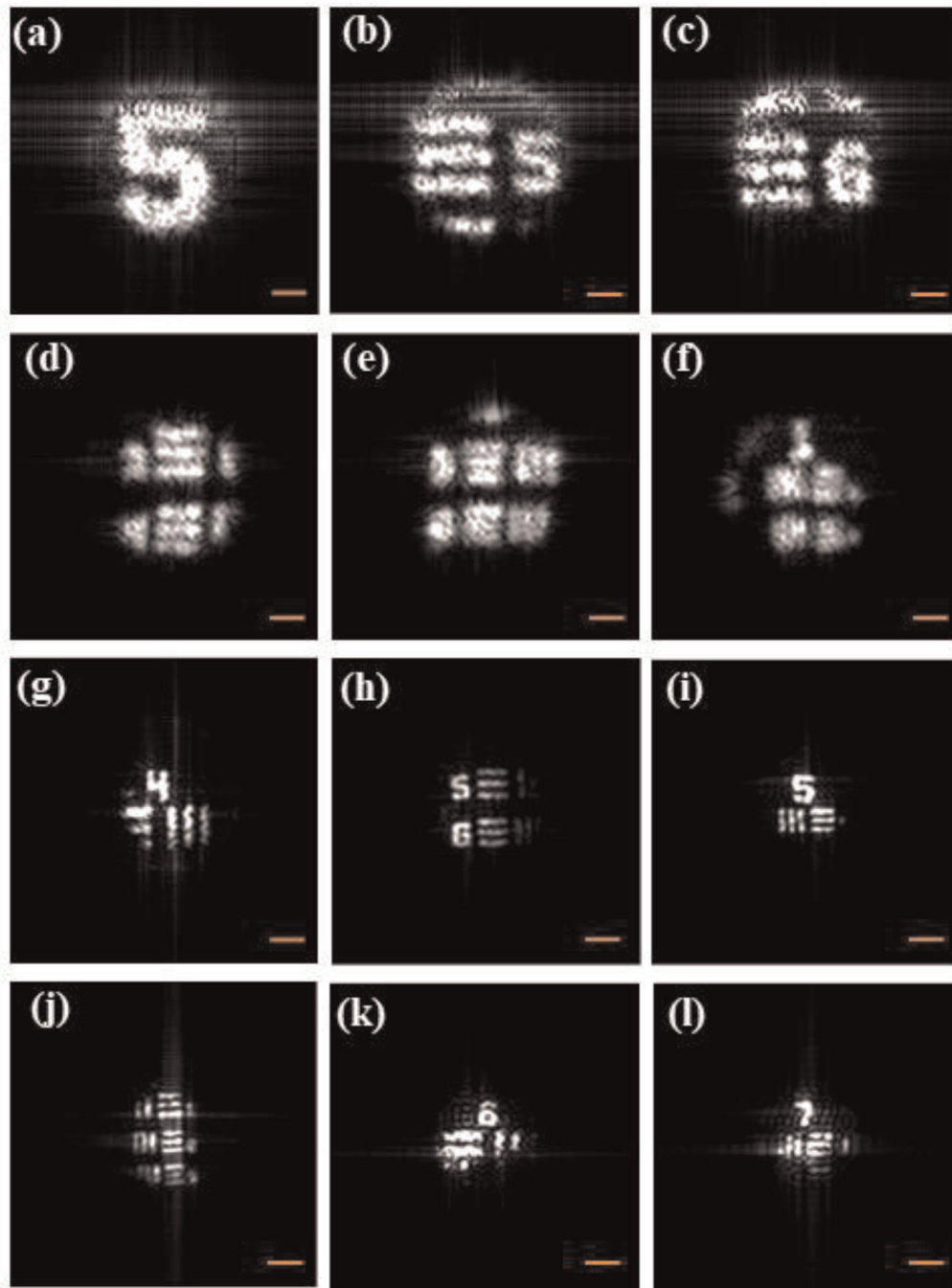


Figure 9. Quantitative imaging results of GDH and GDHM system with negative 1951 USAF resolution test target as sample. Recovered amplitude distributions: (a) group -2 element 5, (b) group -1 element 5, (c) group -1 element 6, (d) group 0 element 3-4, (e) group 0 element 5-6, & (f) group 1 element 1; GDHM system: (g) group 4 element 1, (h) group 4 element 5-6, (i) group 5 element 1, (j) group 5 element 1-3, (k) group 6 element 1 & (l) group 7 element 1. Scale bar: (a)-(f) 1.15 mm, (g)-(j) 57.5 μm , (k) 23.0 μm , and (l) 11.5 μm . Adapted with permission from [36] © The Optical Society.

sorting of incoherent optical vortex modes [65]. This section describes the recently developed technique for OAM mode detection and characterization by exploiting the potential features of GDH system. The technique exploits the properties of speckle field to encode and transmit the OAM modes. The holography assisted GD scheme is utilized for simultaneous detection of amplitude and phase of the OAM modes, and thereby provides an additional feature of determining the helicity of the various modes.

Imaging system	System specifications			Reconstruction area in USAF resolution target	Reconstruction limit	
	MO	L (mm)	M		Line pairs/mm	Line width (μm)
GDH			1	G0-E4	1.41	355
GDHM	40X/ 0.65NA	100	20	G4-E6	28.50	17.5
	60X/ 0.85NA	100	30	G5-E3	40.30	12.4
	100X/ 1.25NA	100	50	G6-E2	71.80	7.0
	100X/ 1.25NA	200	100	G7-E1	128.0	3.9

M: Magnification; MO: Microscope Objective; L: Tube Lens; G: Group; and E: Element.
 Adapted with permission from [36] © The Optical Society.

Table 1.
 Quantitative analysis on the imaging system.

4.1 Generation and recovery of OAM modes with GDH

The applicability of the GDH technique in the generation and recovery of OAM modes is demonstrated with the experimental system shown in **Figure 10**. The light from a coherent light source splits into two parts by a non-polarized beam splitter (BS1), where the transmitted part passes through a rotating ground glass diffuser (GG1) controlled by an aperture (A) of specific size and generates a spatially incoherent light beam with random speckle field at each instant of time. The random field from the rotating ground glass illuminates the reflecting type of phase sensitive SLM, which is used to encode different vortex modes with specific l values. The vortex

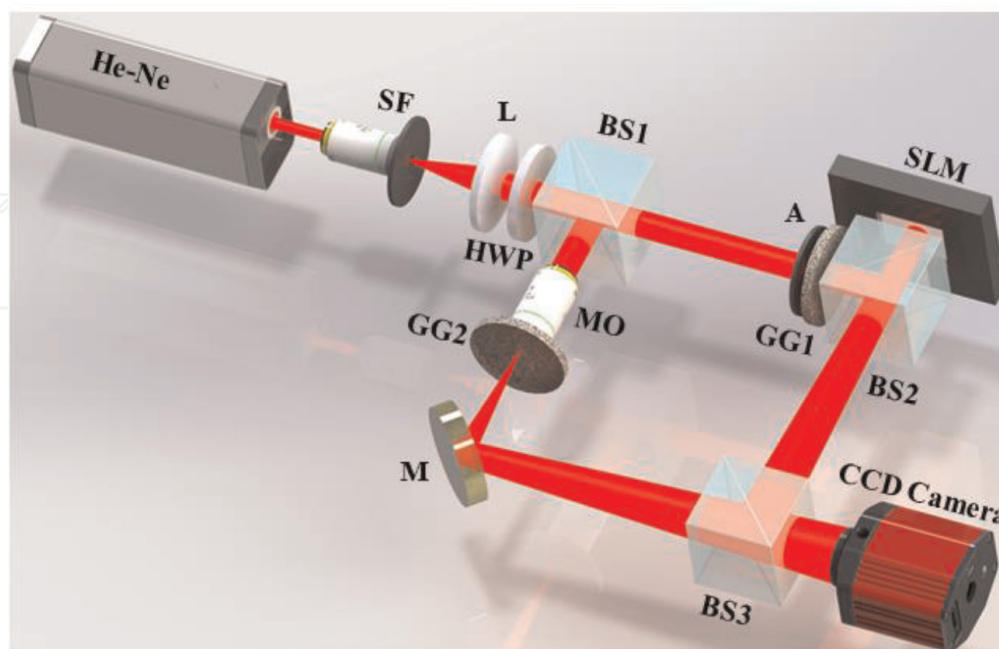


Figure 10.
 Schematic of the experimental design of the GDH system for the generation and recovery of OAM modes; He-Ne: helium-neon laser source; M: mirror; SF: spatial filter assembly; L: lens; HWP: half wave plate; A: aperture; GG: ground glass diffuser; BS: beam splitter; SLM: spatial light modulator; MO: microscope objective; and CCD: charge coupled device camera. Adapted from [50].

mode encodes in the speckle field generated from the diffuser, and the field distribution in a transverse plane at a distance z from the diffuser plane is given by,

$$\psi_1(r) = \frac{\exp(ikz)}{i\lambda z} \int \psi_0(\hat{r}) \exp(i\varphi_g(\hat{r})) V_0^{el}(\hat{r}) \exp\left[\frac{ik}{2z}(|r|^2 - 2r \cdot \hat{r} + |\hat{r}|^2)\right] d\hat{r} \quad (12)$$

where $\psi_0(\hat{r})$ is the incident light field at the exit plane of the diffuser, $\varphi_g(\hat{r})$ the random phase introduced by the ground glass diffuser, $V_0^{el}(\hat{r}) = \exp(i\epsilon l \phi)$ the vortex mode with zero radial index and l azimuthal index, where ϵ and l represent the sign and magnitude of the TC of the specific OAM mode, λ the wavelength of the light source, $k = 2\pi/\lambda$ the wave number of light, z the propagation distance, and \hat{r} and r are the position coordinates at the source plane and detector plane, respectively.

The holographic random field for the GD scheme is achieved by making an off axis point source illumination on an independent diffuser (GG2) in the reflected beam from BS1. The reference random field generated from the diffuser in the holographic arm is given by,

$$\psi_R(r) = \frac{\exp(ikz)}{i\lambda z} \int \psi_R(\hat{r}) \exp(i\varphi_R(\hat{r})) \exp\left[\frac{ik}{2z}(|r|^2 - 2r \cdot \hat{r} + |\hat{r}|^2)\right] d\hat{r} \quad (13)$$

where $\psi_R(\hat{r})$ is the incident light field at the exit plane of the diffuser, $\varphi_R(\hat{r})$ the random phase introduced by the diffuser in the holographic arm. This reference random field propagates and combines independently with the specific vortex encoded spatially incoherent field from the SLM arm. The technique utilizes a sequential snapshot recording of the time frozen speckle fields corresponding to various modes and the recording is implemented using a CCD, which is synchronized with GG1 and SLM. The approach exploits the spatial averaging as a replacement of ensemble averaging in the execution of digital cross-correlation of recorded intensity fluctuations at the detector plane [36, 37, 42].

With the assumption of the scattered field from the diffusers obeys the Gaussian statistics and by utilizing the fourth order moment of the field at the detector plane [39, 40], the correlation of intensity fluctuations is expressed in terms of the respective second order correlation function as,

$$\langle \Delta I_m(r_1) \Delta I_0(r_2) \rangle = |W(r_1, r_2) + W^R(r_1, r_2)|^2 \quad (14)$$

with $\langle \dots \rangle$ represents the ensemble averaging, $I_m(r_1) = (\psi_m(r_1) + \psi_R(r_1))^*$ $(\psi_m(r_1) + \psi_R(r_1))$ the resultant intensity contribution from $\psi_m(r)$ and $\psi_R(r)$, $I_0(r_2) = (\psi_0(r_2) + \psi_R(r_2))^* (\psi_0(r_2) + \psi_R(r_2))$ the resultant intensity contribution from $\psi_0(r)$ and $\psi_R(r)$ with m representing any positive integer, $\Delta I_m(r_1) = I_m(r_1) - \langle I_m(r_1) \rangle$, $\Delta I_0(r_2) = I_0(r_2) - \langle I_0(r_2) \rangle$ represents the fluctuation of the intensity value with respect to its average value for the respective intensity distributions at the detector plane, $W(r_1, r_2) = \langle \psi_m^*(r_1) \psi_0(r_2) \rangle$, and $W^R(r_1, r_2) = \langle \psi_R^*(r_1) \psi_R(r_2) \rangle$ are the second order correlation functions corresponding to vortex encoded field and a reference random field, respectively. Here, we are justified in taking the contribution from the cross terms zero. i.e., $\langle \psi_m^*(r_1) \psi_R(r_2) \rangle = \langle \psi_R^*(r_1) \psi_0(r_2) \rangle = 0$, since independent diffusers are used to generate the respective random fields. Eq. (14) describes that the

intensity correlation at the detector plane results in to a ‘correlation hologram’, which is the result of the superposition of second order complex field correlation functions [36, 43, 44].

For a fixed wavelength λ and at a fixed propagation distance z , by considering $\hat{r}_2 = \hat{r}_1 = \hat{r}$, $r_1 = r + \Delta r$, $r_2 = r$, and $\Delta r = r_1 - r_2$; the recovered complex cross-correlation function is expressed as,

$$\mathbf{W}(\Delta r) \propto \int I_0(\hat{r}) V_0^{el}(\hat{r}) \exp \left[-i \frac{2\pi}{\lambda z} \Delta r \cdot \hat{r} \right] d\hat{r} \quad (15)$$

where $I_0(\hat{r}) = \psi_0^*(\hat{r})\psi_0(\hat{r})$ represents the non-stochastic intensity distribution at the diffuser plane. The correlation function $\mathbf{W}(\Delta r)$ is directly related to the intensity distribution at the diffuser plane $I_0(\hat{r})$ and the encoded vortex phase information $V_0^{el}(\hat{r})$ at the exit plane of the diffuser. In a similar way, the reference correlation function $W^R(\Delta r)$ is considered as,

$$W^R(\Delta r) \propto \int I_R(\hat{r}) \exp \left[-i \frac{2\pi}{\lambda z} \Delta r \cdot \hat{r} \right] d\hat{r} \quad (16)$$

where $I_R(\hat{r}) = \text{circ}\left(\frac{\hat{r}-r_s}{a}\right)$ is the intensity distribution at the reference diffuser GG2, which is utilized in the GDH system for the generation of the correlation hologram. i.e., the intensity of the reference field at off-axis position ' r_s ' and size ' a ' of the circular aperture. The reference random field is created by an off axis point source illumination on GG2 with an aperture size ' a ' and position ' r_s ', which generates a linear phase that support the recording of the correlation hologram.

A digital recovery process utilizing Fourier domain filtering approach [46] retrieves the complex correlation function $\mathbf{W}(\Delta r)$ from other redundant terms in Eq. (14). The retrieval of the complex correlation function offers a new detection scheme for the OAM modes scrambled in the speckle pattern. The retrieval of phase distribution along with the amplitude of the OAM modes with the GDH system delivers a direct scheme for the simultaneous determination of sign and magnitude of the topological charge of specific helicity. An anticlockwise helical structure direction represents the positive sign of the TC, and a clockwise helical structure direction represents a negative TC for the recovered OAM modes.

4.2 Recovered OAM modes

The GDH system assisted with SLM is utilized to encode phase masks corresponding to various TC. The sequential encoding of specific phase mask in the SLM and illumination with the random light from the rotating diffuser generate the vortex encoded speckle fields with various OAM modes. The corresponding intensity distributions of speckle patterns were recorded with CCD for various position shifts of the rotating diffuser. The intensity distribution of resultant speckle patterns obtained with specific topological charges are shown in **Figure 11a–d** and the respective reference speckle patterns are shown in **Figure 11e–h**. The inset of **Figure 11** shows the enlarged view of the marked specific region, where in **Figure 11a–d** clearly represents the speckle pattern modulation with interference fringes corresponding to various vortex phase masks in comparison to the inset images of **Figure 11e–h** of reference speckle intensity distributions.

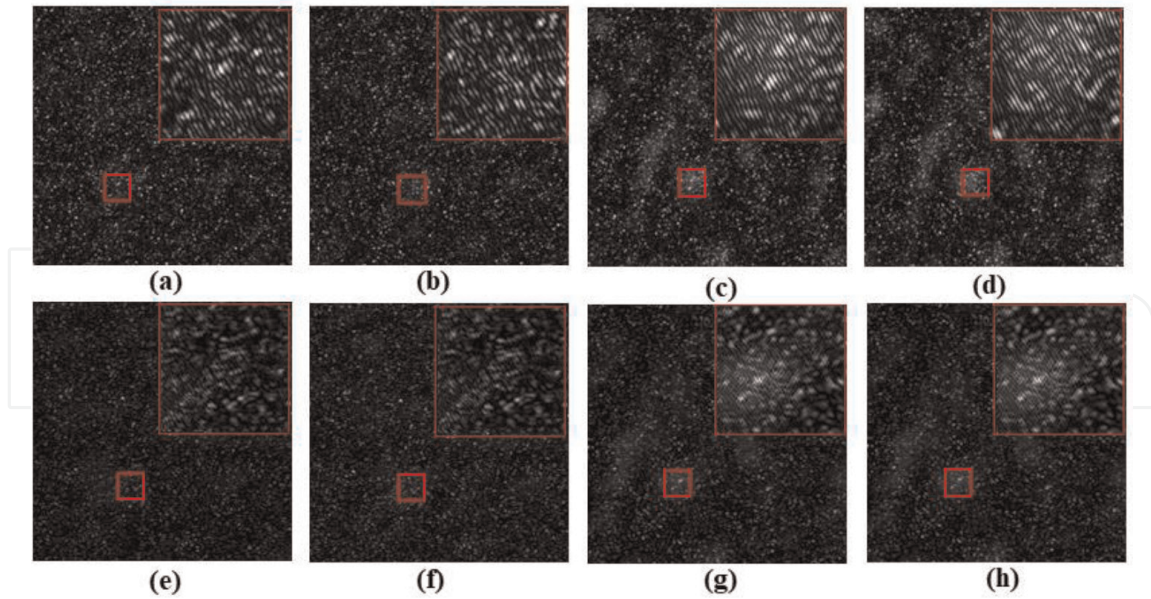


Figure 11.

(a–d) CCD recorded resultant speckle intensity distribution for OAM modes with $l = 1, 4, -1$ & -4 , respectively; (e–h) CCD recorded resultant speckle intensity distribution for respective reference speckle field.

The cross-correlation of CCD recorded intensity fluctuations based on spatial averaging retrieves the correlation hologram at the detector plane. The retrieved correlation hologram corresponding to $el = +1$ & -1 and $el = +4$ & -4 are shown in **Figure 12a–d**. A digital recovery scheme utilizing Fourier transform method of fringe analysis [46] recovers the complex field distribution corresponding to various OAM modes. The recovered amplitude and phase distributions of the vortex modes for respective topological charges are shown in **Figure 12e–l**. The performance of the technique is validated by simulation for various vortex modes with specific helicity and TC by generating a spatially incoherent light source by illuminating a random diffuser with a collimated coherent light source of wavelength 632.8 nm and a beam size of 6.5 mm. The respective simulation results corresponding to $el = +1$ & -1 and $el = +4$ & -4 are shown in **Figure 13a–l**. The simultaneous recovery of both phase and amplitude distributions corresponding to specific OAM modes provides direct advantage of the quantitative determination of magnitude and sign of the topological charge of the generated OAM modes on evaluation of the recovered phase. The recovered phase distributions shown in **Figure 12i–l** in experiment and **Figure 13i–l** in simulation exhibit a phase variation around the singularity in the order of $2l\pi$ with the number of phase jumps equal to the value of l . In addition, the quantitative analysis on the recovered phase distribution allows the direct estimation of the sign of the TC of OAM modes based on the direction of rotation of helicity of the respective modes. An anticlockwise rotation of phase distribution as shown in **Figure 12i–k** and **Figure 13i** and **k** corresponds to positive TC and a clockwise rotation of phase distribution as shown in **Figure 12j** and **l** and **Figure 13j** and **l** corresponds to negative TC of OAM modes.

4.3 Characterization of OAM modes

Furthermore, the recovered OAM modes were characterized by performing a quantitative analysis by making use of the orthogonal projection method [66–68].

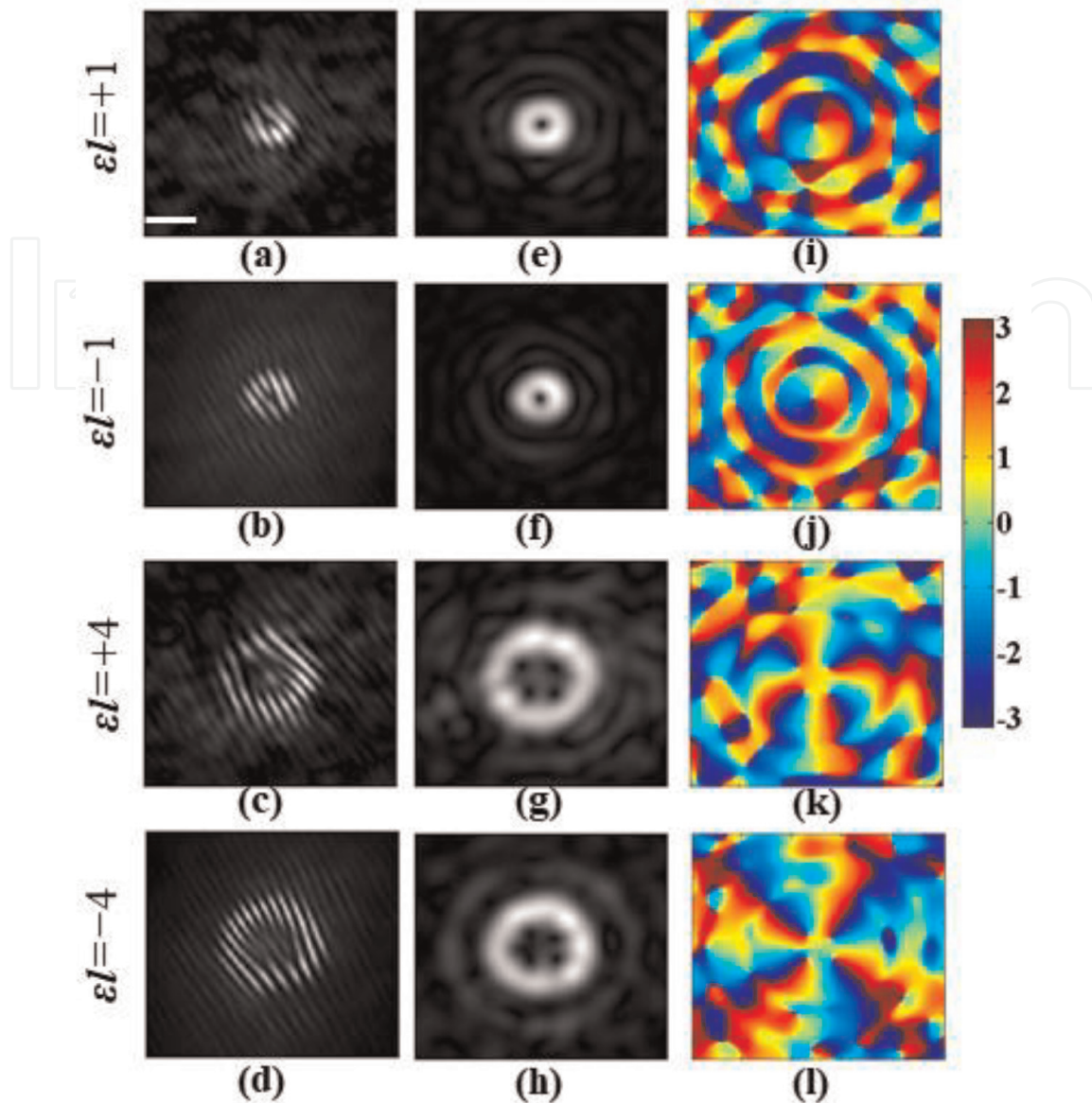


Figure 12.

Experimental results: (a–d) retrieved correlation holograms; (e–h) recovered amplitude distributions of the OAM modes; and (i–l) recovered phase distributions of the OAM modes; scale bar: 110 μm . Adapted from [50].

The projection techniques were utilized to examine the angular momentum associated the field distribution of the light beam. The OAM modes encoded in the recovered correlation function is examined by projecting into respective spiral harmonics $\exp(il\phi)$. The determination of OAM power spectrum gives the provision of decomposition of each OAM components in terms of azimuthal modes. The simulation and experimental results corresponding to the orthogonal projection analysis shown in **Figure 14a–h**, respectively, which exhibits a good agreement. Moreover, an experimental recovery and characterization is performed with the GDH system for OAM modes with different TCs $|\epsilon l| = 1$ to 11, and the quantitative characterization results of respective OAM modes are represented in the plot shown in **Figure 14**. The plot illustrates the experimentally generated OAM modes of $|\epsilon l| = 1$ to 11 and their respective simulation results. The inner and outer radii of OAM modes were retrieved from the respective amplitude distribution of correlation function corresponding to various TCs recovered using the GDH system. The direct dependence of doughnut structure of the amplitude distribution of OAM mode is demonstrated in the plot. The variation of inner and outer radii of

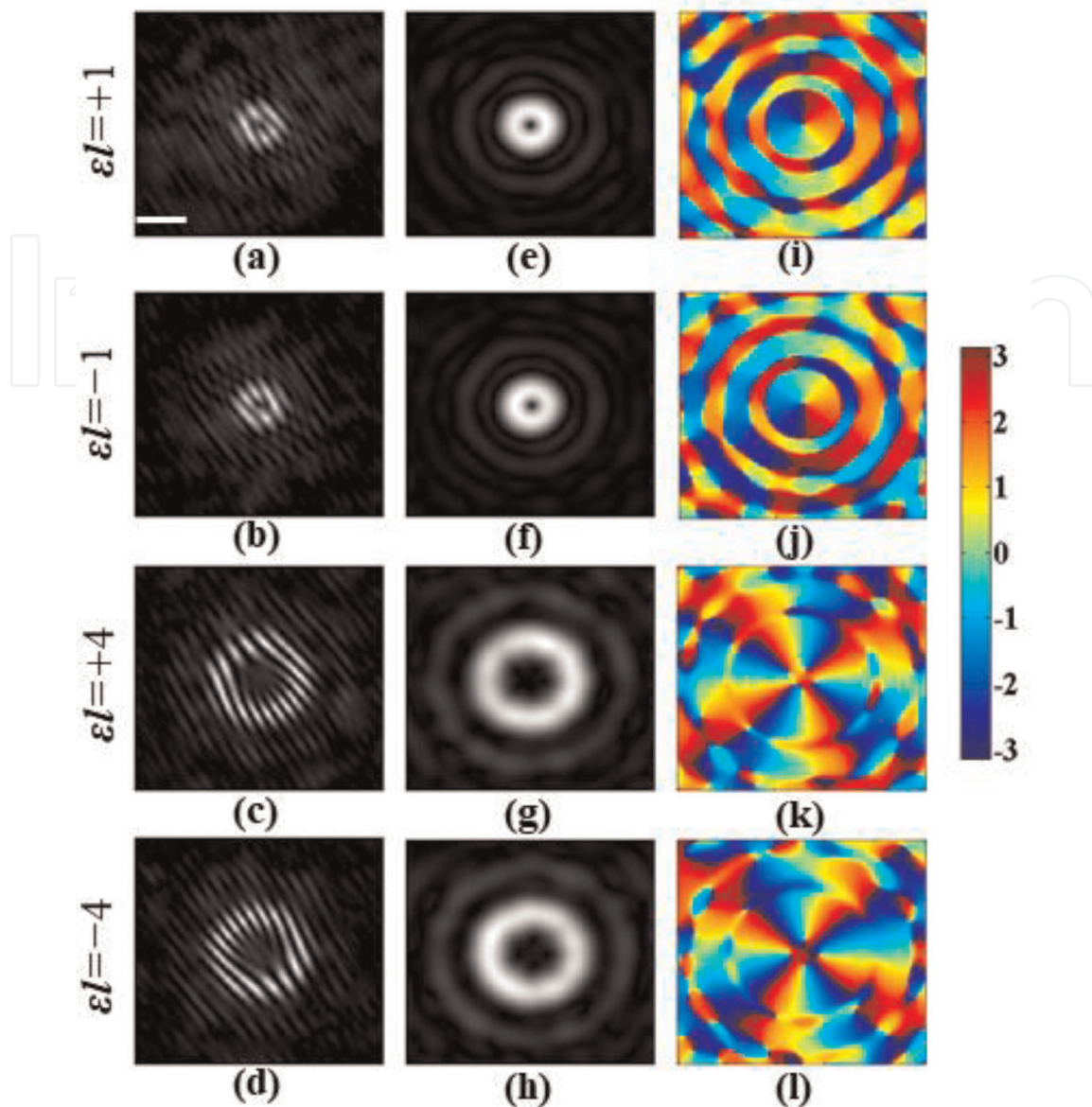


Figure 13. Simulation results: (a–d) retrieved correlation holograms; (e–h) recovered amplitude distributions of the OAM modes; and (i–l) recovered phase distributions of the OAM modes; scale bar: $110 \mu\text{m}$. Adapted from [50].

the recovered modes with various TC are shown in **Figure 15a**, and the variation of areas of dark core and the annular bright rings of the doughnut structure with the TC are shown in **Figure 15b**. The dark core and the annular bright ring have a direct relation with the order of the OAM mode, where an increase in the order of the vortices makes a corresponding increase in the areas of the recovered OAM mode distribution. A good agreement is observed in the quantitative comparison of experimental and theoretical results for all the recovered modes with various l values, which highlight the potential of the technique in recovery and characterization of any OAM modes.

5. Discussion and summary

The development of unconventional correlation assisted GDH design capable of simultaneous detection of ghost diffraction intensity distribution by synchronizing

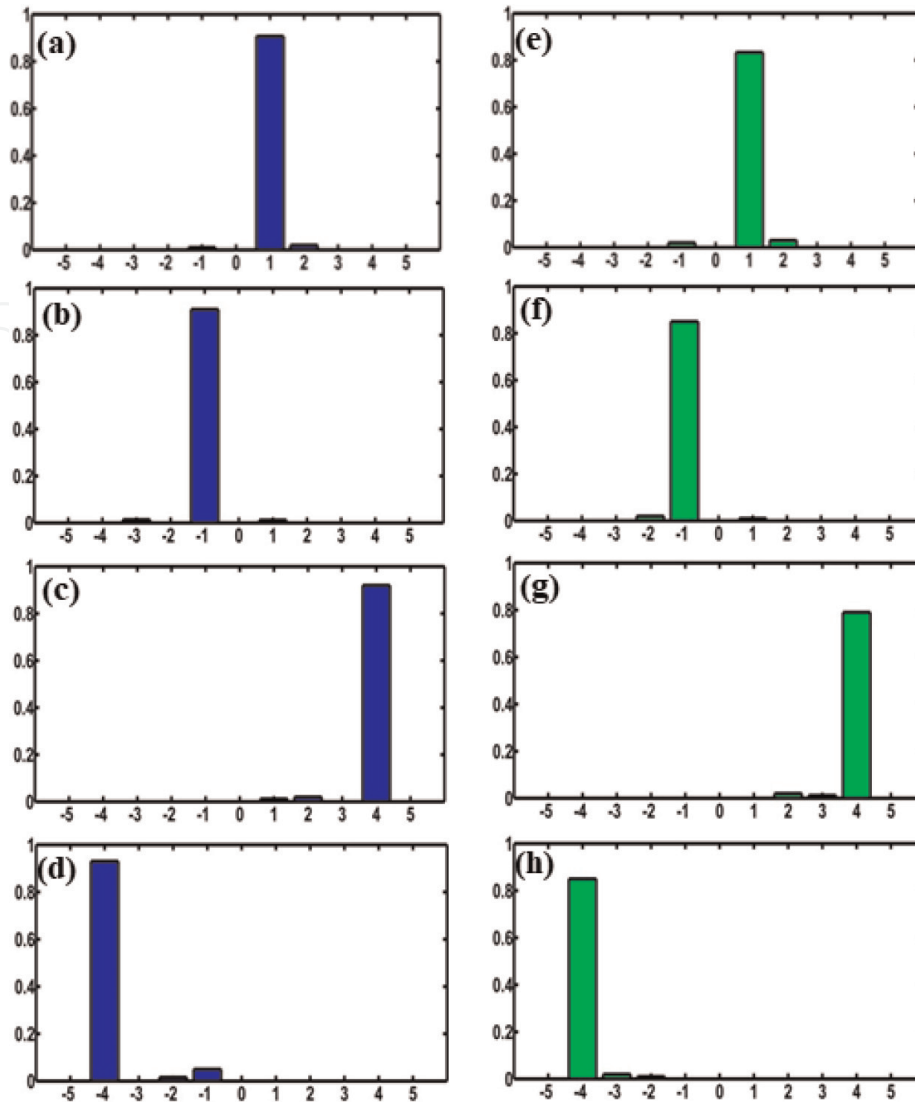


Figure 14. OAM distribution with X-axis the topological charge (ℓ) and Y-axis the OAM power spectrum ($P(\ell)$); (a)–(d) simulation results; and (e)–(h) experimental results.

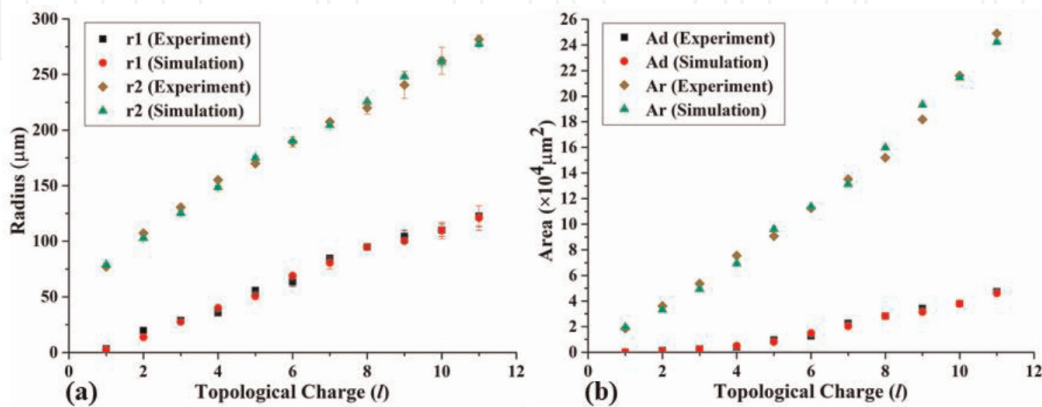


Figure 15. Quantitative comparison of experimental and simulation results of various OAM modes recovered using GDH system: (a) variation of inner and outer radii with the topological charge (r_1 , inner radius and r_2 , outer radius); (b) variation of area of dark core (A_d , dark core) and area of bright annular ring (A_r , annular ring) of the recovered OAM modes. Adapted from [50].

the detectors and recording at an instant of time expands the applied domain of ghost schemes to quantitative phase imaging. The GDH system exploits the wide-sense spatial stationarity of the scattered fields at the detector plane and implements the spatial averaging approach as a replacement of ensemble averaging in the execution of correlation of intensity fluctuations. In recent times, a significant number of research efforts in correlation-based imaging and characterization techniques utilizes the potential features of spatial statistical optics [41, 43, 69–74], but the approach has only very few executions in ghost scenarios [29]. The utilization of spatial averaging provides the potential opportunity to develop the snapshot GDH system, where the single shot detection of two intensity distributions corresponding to the ghost diffraction fields are sufficient to retrieve the ghost correlation hologram, thereby the simultaneous quantitative phase and amplitude imaging.

The extension of the GDH design to the domain of microscopy for imaging of spatially varying complex-valued objects with high-speed and high spatial resolution configurations enlarge the application of the system to quantitative phase microscopy with potential implications in biomedical imaging. Moreover, the spatial resolution of the microscopy system is not only governed by the numerical aperture of the microscopy configuration but also influence on the size of the speckle grains illuminating the object. The design of GDHM system consisting of a variable aperture placed at the rotating diffuser plane controls the beam size illuminating the diffuser, and thereby ensure the proper speckle grain size to improve the resolution of the system. Furthermore, the complex-correlation function recovery feature of the GDH system is exploited to develop a new basis for the recovery of OAM modes encoded in a spatially incoherent random field. The OAM mode propagation and recovery challenge in inhomogeneous or turbulent atmosphere is tackled by exploiting the robust propagation characteristics of spatially incoherent speckle field generated from the pseudo-thermal source, and designing a holography assisted GD scheme with simultaneous determination of amplitude and phase of the encoded vortex modes.

In this chapter, we have presented the recent advancements in the ghost scenarios with the adoption of an unconventional correlation assisted holography scheme for complex-valued object imaging and characterization. The quantitative imaging feature of the GDH technique in comparison to other ghost approaches is established both theoretically and experimentally by imaging of various spatially varying macroscopic and microscopic samples. The implementation of spatial averaging with time-frozen intensity patterns to retrieve the ghost correlation hologram provides the advantage of the real-time imaging with new application dimensions in holography, microscopy, and tomography. Finally, the utilization of GDH scheme for the quantitative recovery of scrambled OAM modes encoded in the random speckle pattern is expected to find significant applications in sorting of superposed optical vortex modes, optical communication, multi-dimensional imaging, quantum and classical information processing, imaging through turbid media, etc.

Acknowledgements

Support from the National Natural Science Foundation of China (NSFC) under grant 12150410318.

IntechOpen

Author details


Vinu Raveendran Pillai Vasantha Kumari^{1*}, Ziyang Chen¹, Rakesh Kumar Singh² and Jixiong Pu¹

1 College of Information Science and Engineering, Fujian Provincial Key Laboratory of Light Propagation and Transformation, Huaqiao University, Xiamen, China

2 Laboratory of Information Photonics and Optical Metrology, Department of Physics, Indian Institute of Technology (BHU), Varana, India

*Address all correspondence to: vinurv@hqu.edu.cn

IntechOpen

© 2022 The Author(s). Licensee IntechOpen. This chapter is distributed under the terms of the Creative Commons Attribution License (<http://creativecommons.org/licenses/by/3.0>), which permits unrestricted use, distribution, and reproduction in any medium, provided the original work is properly cited. 

References

- [1] Padgett M, Aspden R, Gibson G, et al. Ghost imaging. *OPN*. 2016;**27**:38-45
- [2] Hoenders BJ. Review of a bewildering classical-quantum phenomenon: Ghost imaging. In: *Advances in Imaging and Electron Physics*. Vol. 208. San Diego: Academic Press Inc.; 2018. pp. 1-41
- [3] Shapiro JH, Boyd RW. The physics of ghost imaging. *Quantum Information Processing*. 2012;**11**:949-993
- [4] Shih Y. The physics of turbulence-free ghost imaging. *Technologies*. 2016; **4**:39
- [5] Padgett MJ, Boyd RW. An introduction to ghost imaging: Quantum and classical. *Philosophical Transactions of the Royal Society A: Mathematical, Physical and Engineering Sciences*. 2017; **375**:20160233
- [6] Moreau P-A, Toninelli E, Gregory T, et al. Ghost imaging using optical correlations. *Laser Photonics Reviews*. 2018;**12**:1700143
- [7] Ryzkowski P, Barbier M, Friberg AT, et al. Ghost imaging in the time domain. *Nature Photonics*. 2016;**10**: 167-170
- [8] Janassek P, Blumenstein S, Elsässer W. Ghost spectroscopy with classical thermal light emitted by a Superluminescent diode. *Physical Review Applied*. 2018;**9**:1-6
- [9] Shapiro JH. Computational ghost imaging. *Physical Review A*. 2008;**78**: 61802
- [10] Devaux F, Moreau P-A, Denis S, et al. Computational temporal ghost imaging. *Optica*. 2016;**3**:698
- [11] Erkmen BI, Shapiro JH. Ghost imaging: From quantum to classical to computational. *Advances in Optics and Photonics*. 2010;**2**:405-450
- [12] Belinskii A, v, Klyshko DN. Two-photon optics: Diffraction, holography, and transformation of two-dimensional signals. *Journal of Experimental and Theoretical Physics*. 1994;**78**:259-262
- [13] Pittman TB, Shih YH, Strekalov D v, et al. Optical imaging by means of two-photon quantum entanglement. *Physical Review A* 1995; **52**: R3429-R3432.
- [14] Gatti A, Brambilla E, Bache M, et al. Ghost imaging with thermal light: Comparing entanglement and classical correlation. *Physical Review Letters*. 2004;**93**:93602
- [15] Ferri F, Magatti D, Gatti A, et al. High-resolution ghost image and ghost diffraction experiments with thermal light. *Physical Review Letters*. 2005;**94**: 183602
- [16] Borghi R, Gori F, Santarsiero M. Phase and amplitude retrieval in ghost diffraction from field-correlation measurements. *Physical Review Letters*. 2006;**96**:183901
- [17] Duarte MF, Davenport MA, Takhar D, et al. Single-pixel imaging via compressive sampling. *IEEE Signal Processing Magazine*. 2008;**25**:83-91
- [18] He Y, Wang G, Dong G, et al. Ghost imaging based on deep learning. *Scientific Reports*. 2018;**8**:6469
- [19] Rizvi S, Cao J, Zhang K, et al. DeepGhost: Real-time computational ghost imaging via deep learning. *Scientific Reports*. 2020;**10**:11400

- [20] Ferri F, Magatti D, Lugiato LA, et al. Differential ghost imaging. *Physical Review Letters*. 2010;**104**:253603
- [21] Losero E, Ruo-Berchera I, Meda A, et al. Quantum differential ghost microscopy. *Physical Review A*. 2019; **100**:63818
- [22] Li Y-X, Yu W-K, Leng J, et al. Pseudo-thermal imaging by using sequential-deviations for real-time image reconstruction. *Optics Express*. 2019;**27**:35166-35181
- [23] Kingston Andrew M, Pelliccia D, Rack A, et al. Ghost tomography. *Optica*. 2018;**5**:1516-1520
- [24] Pelliccia D, Rack A, Scheel M, et al. Experimental X-ray ghost imaging. *Physical Review Letters*. 2016; **117**:113902
- [25] Olbinado MP, Paganin DM, Cheng Y, et al. Phase-sensitive x-ray ghost imaging. 2019
- [26] Li S, Cropp F, Kabra K, et al. Electron ghost imaging. *Physical Review Letters*. 2018;**121**:114801
- [27] Khakimov RI, Henson BM, Shin DK, et al. Ghost imaging with atoms. *Nature*. 2016;**540**:100-103
- [28] Abouraddy AF, Stone PR, Sergienko AV, et al. Entangled-photon imaging of a pure phase object. *Physical Review Letters*. 2004;**93**:213903
- [29] Bache M, Magatti D, Ferri F, et al. Coherent imaging of a pure phase object with classical incoherent light. *Physical Review A*. 2006;**73**:53802
- [30] Zhang M, Wei Q, Shen X, et al. Lensless Fourier-transform ghost imaging with classical incoherent light. *Physical Review A*. 2007;**75**:21803
- [31] Gong W, Han S. Phase-retrieval ghost imaging of complex-valued objects. *Physical Review A*. 2010;**82**: 23828
- [32] Zhang DJ, Tang Q, Wu TF, et al. Lensless ghost imaging of a phase object with pseudo-thermal light. *Applied Physics Letters*. 2014;**104**:121113
- [33] Shirai T, Friberg AT. Ghost Mach-Zehnder interferometry for phase measurement with spatially incoherent light. *Journal of Optics*. 2020;**22**:045604
- [34] Clemente P, Durán V, Tajahuerce E, et al. Single-pixel digital ghost holography. *Physical Review A*. 2012;**86**: 41803
- [35] Shirai T, Setälä T, Friberg AT. Ghost imaging of phase objects with classical incoherent light. *Physical Review A*. 2011;**84**:41801
- [36] Vinu RV, Chen Z, Singh RK, et al. Ghost diffraction holographic microscopy. *Optica*. 2020;**7**:1697-1704
- [37] Huang Y, Chen Z, et al. Snapshot ghost diffraction imaging based on spatial averaging. *Proceedings of SPIE. Advanced Optical Imaging Technologies IV*. 2021;**11896**:16-21. DOI: 10.1117/122600803
- [38] Singh RK, Vinu RV, Chen Z, et al. Quantitative phase recovery in ghost imaging. In: 2021 IEEE Photonics Conference, IPC Proceedings, Vancouver. 2021. DOI: 10.1109/IPC48725.2021.9592877
- [39] Goodman JW. *Speckle Phenomena in Optics: Theory and Applications*. Englewood: Coberts &Co; 2007
- [40] Goodman JW. *Statistical Optics*. NJ: Wiley-Interscience; 2000. DOI: 10.1017/CBO9781107415324.004

- [41] Takeda M, Wang W, Naik DN, et al. Spatial statistical optics and spatial correlation holography: A review. *Optical Review*. 2014;**21**:849-861
- [42] Takeda M. Spatial stationarity of statistical optical fields for coherence holography and photon correlation holography. *Optics Letters*. 2013;**38**: 3452-3455
- [43] Singh RK, Vyas S, Miyamoto Y. Lensless Fourier transform holography for coherence waves. *Journal of Optics*. 2017;**19**:115705
- [44] Singh RK, Vinu RV, Sharma MA. Recovery of complex valued objects from two-point intensity correlation measurement. *Applied Physics Letters*. 2014;**104**:111108
- [45] Vinu RV, Singh RK. Determining helicity and topological structure of coherent vortex beam from laser speckle. *Applied Physics Letters*. 2016;**109**: 111108
- [46] Takeda M, Ina H, Kobayashi S. Fourier-transform method of fringe-pattern analysis for computer-based topography and interferometry. *Journal of the Optical Society of America*. 1982; **72**:156-160
- [47] Goodman JW. *Introduction to Fourier Optics*. New York: McGraw-Hill; 1996
- [48] Vyas S, Senthilkumaran P. Interferometric optical vortex array generator. *Applied Optics*. 2007;**46**: 2893-2898
- [49] Singh RK, Sharma AM, Senthilkumaran P. Vortex array embedded in a partially coherent beam. *Optics Letters*. 2015;**40**: 2751-2754
- [50] Huang Y, Vinu RV, Chen Z, et al. Recovery and characterization of orbital angular momentum modes with ghost diffraction holography. *Applied Sciences*. 2021;**11**:12167
- [51] Yao AM, Padgett MJ. Orbital angular momentum: Origins, behavior and applications. *Advances in Optics and Photonics*. 2011;**3**:161
- [52] Chen R, Zhou H, Moretti M, et al. Orbital angular momentum waves: Generation, detection, and emerging applications. *IEEE Communications Surveys and Tutorials*. 2020;**22**:840-868
- [53] Willner AE, Ren Y, Xie G, et al. Recent advances in high-capacity free-space optical and radio-frequency communications using orbital angular momentum multiplexing. *Philosophical Transactions of the Royal Society A: Mathematical, Physical and Engineering Sciences*. 2017;**375**. DOI: 10.1098/RSTA.2015.0439
- [54] Gori F, Santarsiero M, Borghi R, et al. Partially coherent sources with helicoidal modes. *Journal of Modern Optics*. 1998;**45**:539-554
- [55] Gbur G, Visser TD. Phase singularities and coherence vortices in linear optical systems. *Optics Communications*. 2006;**259**:428-435
- [56] Zeng J, Lin R, Liu X, et al. Review on partially coherent vortex beams. *Frontiers of Optoelectronics*. 2019;**12**:229-248
- [57] Jesus-Silva AJ, Hickmann JM, Fonseca EJS. Strong correlations between incoherent vortices. *Optics Express*. 2012;**20**:19708
- [58] Reddy SG, Prabhakar S, Kumar A, et al. Higher order optical vortices and formation of speckles. *Optics Letters*. 2014;**39**:4364

- [59] Salla GR, Perumangattu C, Prabhakar S, et al. Recovering the vorticity of a light beam after scattering. *Applied Physics Letters*. 2015;**107**:021104
- [60] Yang Y, Mazilu M, Dholakia K. Measuring the orbital angular momentum of partially coherent optical vortices through singularities in their cross-spectral density functions. *Optics Letters*. 2012;**37**:4949
- [61] Lu X, Zhao C, Shao Y, et al. Phase detection of coherence singularities and determination of the topological charge of a partially coherent vortex beam. *Applied Physics Letters*. 2019;**114**:201106
- [62] Wang T, Pu J, Chen Z. Propagation of partially coherent vortex beams in a turbulent atmosphere. *Optical Engineering*. 2008;**47**:036002
- [63] Jesus-Silva AJ, Alves CR, Fonseca EJS. Robustness of a coherence vortex. *Applied Optics*. 2016;**55**:7544-7549
- [64] Chen J, Li Y. Discrimination of incoherent vortex states of light. *Optics Letters*. 2018;**43**:5595
- [65] Bezerra DO, Amaral JP, Fonseca EJS, et al. Sorting of spatially incoherent optical vortex modes. *Scientific Reports*. 2020;**10**:10
- [66] Sarkar T, Parvin R, Brundavanam MM, et al. Higher-order stokes-parameter correlation to restore the twisted wave front propagating through a scattering medium. *Physical Review A*. 2021;**104**:013525
- [67] D'Errico A, Piccirillo B, Cardano F, et al. Measuring the complex orbital angular momentum spectrum and spatial mode decomposition of structured light beams. *Optica*. 2017;**4**:1350-1357
- [68] Molina-Terriza G, Torres JP, Torner L. Management of the Angular Momentum of light: Preparation of photons in multidimensional vector states of angular momentum. *Physical Review Letters*. 2001;**88**:013601
- [69] Naik DN, Singh RK, Ezawa T, et al. Photon correlation holography. *Optics Express*. 2011;**19**:1408-1421
- [70] Takeda M, Singh AK, Naik DN, et al. Holographic Correloscopy-unconventional holographic techniques for imaging a three-dimensional object through an opaque diffuser or via a Scattering Wall: A review. *IEEE Transactions on Industrial Informatics*. 2016;**12**:1631-1640
- [71] Kim K, Somkuwar AS, et al. Imaging through scattering media using digital holography. *Optics Communications*. 2019;**439**:218-223
- [72] Chen L, Chen Z, Singh RK, et al. Increasing field of view and signal to noise ratio in the quantitative phase imaging with phase shifting holography based on the Hanbury Brown-Twiss approach. *Optics and Lasers in Engineering*. 2022;**148**:106771
- [73] Vinu RV, Singh RK. Experimental determination of generalized stokes parameters. *Optics Letters*. 2015;**40**:1227-1230
- [74] Vinu RV, Singh RK. Synthesis of statistical properties of a randomly fluctuating polarized field. *Applied Optics*. 2015;**54**:6491-6497